Fluid Dynamics & Materials Processing

Tech Science Press

http://doi.org/10.32604/fdmp.2026.085657

ARTICLE

Experimental Investigation of Seepage-Induced Rheological Deformation in Mucky Soft Soil Containing Medium-Fine Sand

Longbin Lin[1] and Hua Hu[2,*]

[1]School of Civil Engineering, Xiamen University Tan Kah Kee College, Zhangzhou, China
[2]School of Architecture and Civil Engineering, Xiamen University, Xiamen, China
*Corresponding Author: Hua Hu. Email: xmhuh@xmu.edu.cn

Received: 19 May 2026; Accepted: 15 July 2026; Published: 31 July 2026

ABSTRACT: Seepage-induced rheological deformation represents a critical factor governing the long-term stability of coastal soft-soil excavations subjected to intense rainfall infiltration and groundwater fluctuations. This study elucidates the individual and interactive effects of seepage pressure and seepage duration on the time-dependent deformation behavior of undisturbed mucky soft soil containing medium-fine sand, collected from a deep foundation pit. A comprehensive experimental campaign based on triaxial seepage-shear rheological testing for a confining pressure of 180 kPa is presented, encompassing sixteen combinations of seepage pressure and duration together with a directly measured zero-seepage reference condition. Three replicate specimens are examined for each testing scenario. The results demonstrate that seepage significantly accelerates rheological deformation, with axial strain exhibiting a pronounced nonlinear dependence on both hydraulic loading intensity and exposure duration. Under the most adverse seepage condition considered, namely a seepage pressure of 70 kPa maintained for 120 min, the mean axial strains reach 3.63 ± 0.25% and 10.81 ± 0.71% at deviatoric stresses of 300 and 600 kPa, respectively, compared with only 1.34 ± 0.09% and 4.77 ± 0.20% under zero-seepage conditions. Two-way analysis of variance confirms that seepage pressure, seepage duration, and their combined interaction exert statistically significant control over the rheological response. To further characterize this coupled hydraulic-mechanical behavior, an empirical power-law response-surface model is established to describe the dependence of deformation on seepage conditions. The proposed model exhibits strong predictive capability within the investigated range, yielding coefficients of determination of 0.9488 and 0.8579 and leave-one-condition-out cross-validation Q^2 values of 0.9208 and 0.7371 at deviatoric stresses of 300 and 600 kPa, respectively. The framework is specifically applicable to stable pre-failure deformation regimes and should not be extended to conditions approaching failure, such as those corresponding to a deviatoric stress of 900 kPa.

KEYWORDS: Mucky soft soil containing medium-fine sand; seepage pressure; seepage duration; coupled effect; rheological strain

1 Introduction

Soft soil deposits are widely distributed in coastal regions worldwide, including the southeastern coast of China [1], many coastal areas of Southeast Asia [2,3], and other low-lying coastal regions worldwide. These deposits are commonly characterized by high water content, low shear strength, and significant compressibility. Under hydraulic disturbances induced by monsoon rainfall, groundwater fluctuations, or tidal variations, changes in pore-water pressure may reduce effective stress and accelerate time-dependent deformation of soft soils [4–7]. Under sustained engineering loads, coastal soft soils often exhibit pronounced rheological behavior, and the cumulative deformation may progressively impair the serviceability and safety of geotechnical structures such as foundations, slopes, and excavations [1,8]. Therefore, a clear understanding of the rheological response of soft soils under seepage conditions is essential for stability assessment, deformation prediction, and risk warning in coastal geotechnical engineering.

Extensive efforts have been made to investigate the rheological behavior of soft soils and its governing mechanisms. Existing studies can generally be grouped into three categories. The first category focuses on material modification, in which additives such as nanomaterials [9], geopolymers [10], cement-based binders [11], and olivine [12] are introduced to improve strength, reduce compressibility, and enhance creep resistance. Although such studies are valuable for enhancing engineering performance, they primarily address improvement effects rather than the intrinsic deformation behavior of natural soft soils under complex hydraulic conditions. The second category includes engineering case studies on embankments [13,14], airports [2], roads [15], slopes [16], and foundation pits [3], where the long-term deformation behavior of soft soils has been examined under different loading and environmental conditions. While these studies are highly relevant to practice, most of them emphasize macroscopic deformation responses and provide limited quantitative insight into seepage effects and their time dependence. The third category concerns seepage-coupled investigations, which examine the effects of hydraulic gradient, seepage pressure, dynamic loading, and particle composition on the structure, strength, and deformation of soils and related geomaterials. Previous studies have investigated the rheological response of soft clay under coupled seepage and dynamic loading [17], seepage behavior along clay interfaces [18], the influence of fine-particle content on the rheology of sandy soils [19], the creep characteristics and strain-rate effects of soft clays [8], and nonlinear consolidation–rheology coupling models [20]. Related research has more recently progressed toward quantitative prediction and hydraulic–mechanical coupling analysis. Creep testing and model prediction for clayey soils in land-subsidence areas have improved the quantitative characterization of long-term deformation [21], while nonlinear elastic–plastic–viscous models have further enhanced the prediction of creep behavior in marine soft clay [22]. Seepage–creep investigations of fault rocks have additionally shown that applied stress and water pressure can jointly influence time-dependent deformation [23]. Recent studies have further highlighted that hydraulic responses of porous geomaterials involve both fluid transport characteristics and structural evolution under hydraulic disturbance. Pore-scale seepage prediction studies have demonstrated the role of pore architecture in governing fluid migration behavior [24], while cyclic hydraulic disturbance experiments have revealed progressive structural degradation and irreversible deformation of unconsolidated geomaterials under repeated fluid loading [25]. However, most existing studies still focus on a single hydraulic factor, reconstituted specimens, or specific boundary conditions, and the rheological response of natural undisturbed soft soils under coupled seepage conditions remains insufficiently quantified.

Despite these advances, studies on mucky soft soil containing medium-fine sand, which is commonly encountered in the southeastern coastal area of China, remain limited. This type of soil is characterized by high water content, low strength, and a certain proportion of sandy particles, and its engineering behavior may differ substantially from that of ordinary saturated clay. Under conditions of intense rainfall and groundwater-level fluctuation, its seepage-induced response may be particularly complex. Existing research has mainly focused on the time-dependent deformation of saturated clay or on consolidation–rheology behavior under a single influencing factor. In contrast, systematic experimental investigations into the main effects of seepage pressure and seepage duration, as well as their interaction, are still lacking. In addition, most available rheological models are intended to describe strain–time evolution under a prescribed condition, whereas quantitative comparison and coupled characterization of deformation responses under different seepage conditions remain inadequate. This limitation restricts the engineering evaluation and prediction of seepage-induced rheological deformation in such soils.

To address these gaps, this study investigated undisturbed mucky soft soil containing medium-fine sand collected from a deep foundation pit in Zhangzhou, China, using triaxial seepage–shear rheological tests. A zero-seepage control condition was introduced, and a 4 × 4 factorial design was adopted to systematically examine the individual and combined effects of seepage pressure and seepage duration on axial rheological strain. Replicate-level two-way analysis of variance was then employed to identify the main effects of these two factors and their interaction. Furthermore, for the stable deformation stages at deviatoric stresses of 300 and 600 kPa, an empirical power-function response-surface model was established to quantify the relationship between seepage conditions and final rheological strain. It should be emphasized that this model is not intended as a universally applicable constitutive law; rather, it provides statistically interpretable and engineering-relevant experimental evidence for evaluating seepage-induced rheological deformation of saturated mucky soft soil containing medium-fine sand within the tested range.

2 Materials and Methods

2.1 Sample Collection and Physical Properties

Soil samples were collected from a deep foundation pit project in Zhangzhou, Fujian Province, China. The stratigraphic profile at the site consists, from top to bottom, of: (1) miscellaneous fill, (2) mucky soft soil containing medium-fine sand, (3) medium-fine sand, (4) mucky soft soil containing medium-fine sand, (5) medium-coarse sand, (6) gravel, (7) completely weathered granite, (8) strongly weathered granite, and (9) moderately weathered granite. The tested soil was obtained from Layers ② and ④, which were identified in the geotechnical investigation report as mucky soft soil containing medium-fine sand. These soft soil layers are important to the deformation and stability of the foundation pit under seepage conditions.

Undisturbed soil samples representative of Layers ② and ④ were collected using thin-walled sampling tubes to minimize compression and shear disturbance during extraction. After sampling, both ends of each tube were immediately sealed to prevent moisture loss. The tubes were securely fixed during transportation, and the samples were stored in a sealed environment before specimen preparation. The collected soil was black to brownish gray, exhibited a fluid-plastic consistency, and was naturally saturated.

Particle-size analysis showed that the tested soil was dominated by fine-grained fractions, including silt and clay, while medium-fine sand accounted for approximately 20%–30% of the total mass. The measured particle-size distribution is presented in Fig. 1. These results are consistent with the soil description provided in the geotechnical investigation report. Accordingly, the term "mucky soft soil containing medium-fine sand" is used consistently throughout this paper.

The basic physical and mechanical properties of the tested soil are summarized in Table 1.

Table 1: Basic physical and mechanical properties of the tested soil.

Property	Value
Natural water content ω (%)	68.04
Natural density ρ (g/cm^3)	1.58
Natural void ratio e	1.90
Plasticity index I_p	22.50
Liquidity index I_L	1.59
Cohesion c (kPa)	8.30
Internal friction angle φ (°)	2.97

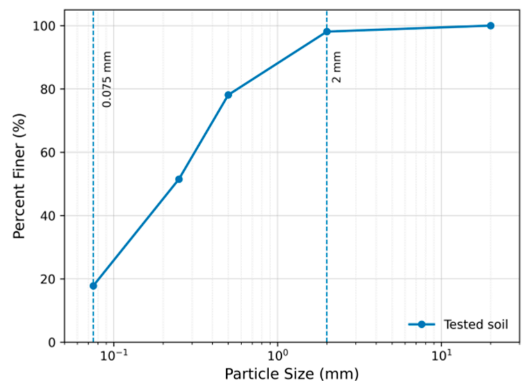

Figure 1: Particle-size distribution of the tested soil.

2.2 Test Apparatus and Procedure

An SLB-1 stress–strain-controlled triaxial seepage–shear apparatus manufactured by Nanjing Soil Instrument Factory was used in this study. Its main technical specifications are listed in Table 2. The apparatus provides both stress and strain control and allows seepage and axial loading to be applied simultaneously. A prescribed seepage-pressure difference can be maintained by independently regulating the water pressures at the inflow and outflow ends of the specimen.

Table 2: Main technical parameters of the SLB-1 triaxial seepage–shear apparatus.

Parameter	Range	Accuracy	Remarks
Axial force	0–20 kN	±1% FS (10%–95% FS)	—
Axial strain-rate control	0.002–4 mm/min	±10%	Constant strain control
Axial stress control	0–20 kN	±1%	Constant stress control
Cell pressure	0–1.99 MPa	±0.5% FS	Set value: 0.01–1.95 MPa
Back pressure	0–0.99 MPa	±0.5% FS	Set value: 0.01–0.99 MPa
Volume change	0–480 mL	—	Digital display

A photograph of the triaxial seepage–shear apparatus is shown in Fig. 2, and the overall experimental procedure is summarized in Fig. 3.

Cylindrical specimens measuring 39.1 mm in diameter and 80 mm in height were carefully trimmed from the tube samples in accordance with GB/T 50123-2019. Each specimen was placed between upper and lower porous stones, enclosed in a rubber membrane, and installed in the triaxial chamber. Back-pressure saturation was then performed until the pore-pressure coefficient B exceeded 0.95, indicating an adequately saturated state. The specimens were subsequently consolidated under drained conditions at a cell pressure of 180 kPa.

After consolidation, the seepage condition was established by controlling the water pressures at the two ends of the specimen. The pressure at the upper end was maintained at 0 kPa, while a prescribed pressure was applied at the lower end, producing an upward and constant seepage-pressure difference across the specimen. The selected seepage condition was maintained for the specified duration before axial rheological loading was initiated.

The specimens were then subjected to drained multistage loading at axial deviatoric stresses of 300, 600, and 900 kPa. Each loading stage was maintained for up to 180 min and was terminated earlier if the deformation approached stabilization or the preset termination condition was reached. This multistage loading scheme was adopted to obtain the rheological responses at different stress levels from the same specimen and thereby reduce the influence of specimen-to-specimen variability.

Figure 2: SLB-1 triaxial seepage–shear apparatus used in this study.

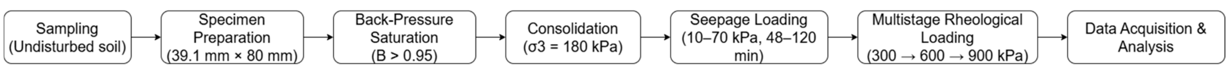

Figure 3: Flowchart of the experimental program and testing procedure.

In accordance with GB/T 50123-2019 and the preset test-control procedure, the test was terminated when the axial strain reached 15% if no distinct peak failure occurred earlier. All specimens reached this termination condition rapidly during the 900 kPa stage. Therefore, the observations at this stage represent termination-limited data at $\varepsilon \geq 15\%$, rather than stable rheological endpoints or exact post-failure strains. The 900 kPa data were consequently excluded from the regression modeling and two-way ANOVA of stable terminal strain. Axial stress, seepage pressure, elapsed time, and axial strain were recorded automatically throughout the tests.

2.3 Test Plan and Parameter Design

The test program was designed to quantify the individual and interaction effects of seepage pressure and seepage duration on the rheological response of undisturbed mucky soft soil containing medium-fine sand. All tests were conducted under saturated and consolidated-drained conditions at a constant cell pressure of 180 kPa. Seepage pressure, seepage duration, and axial deviatoric stress were treated as the principal controlled variables, while the soil type, specimen dimensions, saturation procedure, and consolidation condition were kept unchanged.

Four seepage-pressure levels of 10, 30, 50, and 70 kPa and four seepage-duration levels of 48, 72, 96, and 120 min were selected, producing a 4 × 4 factorial matrix of 16 seepage conditions. These levels were determined based on the operating range of the apparatus, preliminary exploratory tests, and the need to represent progressively increasing hydraulic loading without inducing immediate seepage-related failure before axial loading. In addition, one zero-seepage control condition P = 0 kPa and T = 0 min was tested to directly determine the baseline rheological response. Three replicate specimens were tested under each condition to evaluate experimental repeatability and provide replicate-level data for statistical analysis.

After the prescribed seepage stage, the specimens were subjected to three levels of axial deviatoric stress, namely 300, 600, and 900 kPa. These stress levels were selected from preliminary seepage–shear rheological tests to represent stable deformation at the first two stages and rapid failure at the highest stage. Because all specimens reached the preset termination condition during the 900 kPa stage, only the stable terminal strains obtained at 300 and 600 kPa were used for response-surface modeling and two-way analysis of variance.

The complete test-condition matrix is presented in Table 3. The factorial design enables the main effects of seepage pressure and seepage duration, as well as their interaction, to be evaluated within the tested range.

Table 3: Test-condition matrix for seepage–rheology experiments on undisturbed mucky soft soil containing medium-fine sand.

Condition No.	Seepage Pressure/kPa	Seepage Duration/min	Condition No.	Seepage Pressure/kPa	Seepage Duration/min
0	0	0	9	50	48
1	10	48	10	50	72
2	10	72	11	50	96
3	10	96	12	50	120
4	10	120	13	70	48
5	30	48	14	70	72
6	30	72	15	70	96
7	30	96	16	70	120
8	30	120			

2.4 Data Processing Method

Chen's multistage loading method was used to convert the measured step-loading curves into equivalent single-stage rheological curves [26]. Based on the concepts of material memory and strain superposition, the strain increment generated at each stress step was separated and shifted to reconstruct the response corresponding to the specified deviatoric-stress level. This approach enables rheological responses at several stress levels to be obtained from the same specimen, thereby reducing the number of independent long-duration tests and limiting the influence of specimen-to-specimen variability.

Although saturated mucky soft soil containing medium-fine sand exhibits nonlinear and time-dependent rheological behavior and therefore does not strictly satisfy the assumptions of linear superposition, the applicability of Chen's method depends primarily on the deformation stage under consideration rather than on strict linear viscoelasticity. In the present study, the converted curves were used only for the 300 and 600 kPa loading stages, where the specimens predominantly exhibited attenuated and approximately steady rheological deformation without obvious structural collapse or accelerated creep. Under these conditions, the loading-history memory effect is expected to dominate, whereas the influence of progressive structural degradation remains relatively limited. Therefore, Chen's method provides a reasonable engineering approximation for comparing creep responses under different seepage conditions.

Previous studies have successfully applied Chen's multistage loading method to sedimentary peaty soil [27], coastal soft clay [1], and soda residue soil [28], providing practical evidence for its applicability to soft geomaterials. Nevertheless, because the converted curves were not verified by paired single-stage loading tests in the present study, some uncertainty associated with loading-history effects and material nonlinearity may remain. The converted curves should therefore be regarded as equivalent engineering representations rather than exact linear-viscoelastic responses. To minimize this uncertainty, the 900 kPa stage, in which all specimens rapidly reached the preset failure criterion, was used only to identify rapid failure and was excluded from the regression analysis and statistical evaluation. Direct verification using paired single-stage loading tests would further quantify the conversion uncertainty and therefore deserves future investigation.

The replicate-level terminal axial rheological strains at 300 and 600 kPa were first analyzed using two-way fixed-effects ANOVA, with seepage pressure and seepage duration treated as fixed factors. The zero-seepage control condition was excluded from the factorial ANOVA because it did not belong to the complete 4 × 4 test matrix. No statistical outlier was removed, and all three replicate measurements under each condition were retained in the analysis. The coupled dependence of terminal axial rheological strain on seepage pressure and seepage duration was then characterized using an empirical power-function response-surface model fitted to the mean terminal strains of the 16 seepage conditions, with the measured zero-seepage mean used as the baseline value. Details of model fitting, leave-one-condition-out cross-validation, bootstrap 95% confidence interval estimation, and ±10% local sensitivity analysis are presented in Section 3.6.

3 Results and Analysis

3.1 Processed Rheological Curves and Stage Characteristics

Multistage rheological curves were obtained from triaxial seepage–shear tests conducted under different seepage-pressure and seepage-duration conditions. Chen's multistage loading method was then applied to convert the measured step-loading curves into equivalent single-stage rheological curves at deviatoric stresses of 300, 600, and 900 kPa. For brevity, Fig. 4 presents the processed curves of four representative specimens selected from Conditions 1–4.

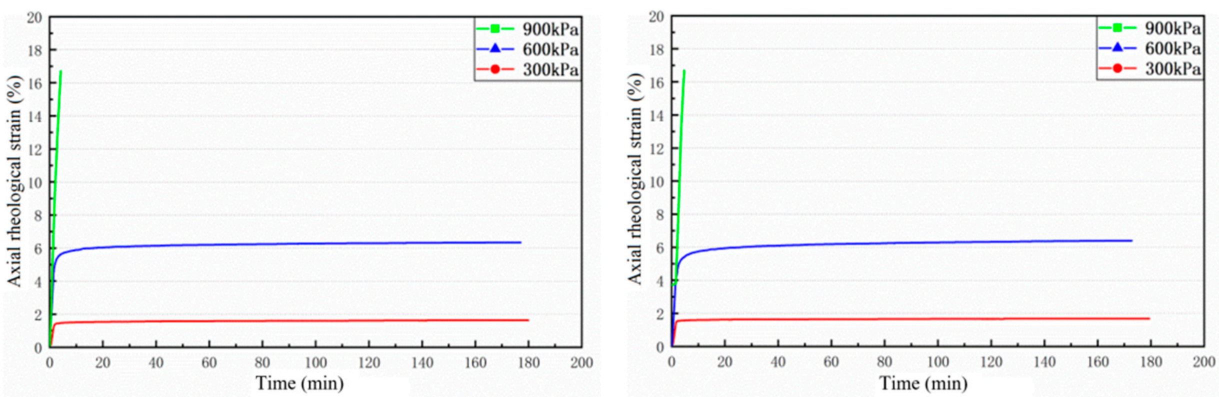

Condition 1 Condition 2

Figure 4: *Cont.*

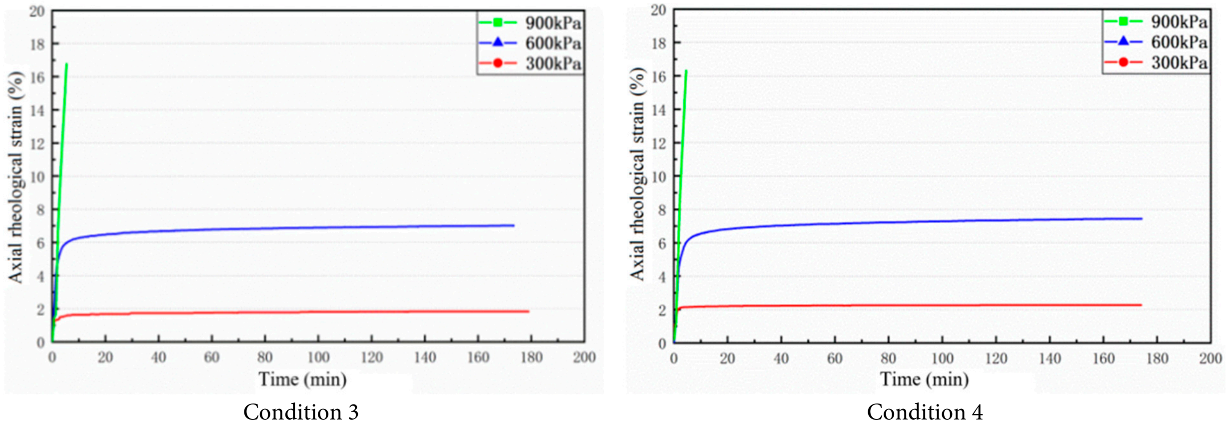

Figure 4: Processed three-stage rheological curves of representative specimens from Conditions 1–4 using Chen's method.

Despite differences in seepage condition, the processed curves exhibit generally similar rheological features. At the beginning of each loading stage, a distinct instantaneous strain was observed. With increasing loading time, the strain–time curves subsequently exhibited three typical stages: attenuated rheology, an approximately steady stage, and accelerated rheology. Similar stage-wise rheological responses have also been reported for other time-dependent geomaterials under sustained loading [5,19].

The main characteristics of these three stages are summarized as follows. (1) Attenuated rheological stage: This stage occurred immediately after loading, during which axial strain continued to increase while the strain increment per unit time decreased rapidly, resulting in a progressively reduced slope of the strain–time curve. (2) Approximately steady rheological stage: The strain increment became very small, and the strain–time curve gradually approached a near-horizontal plateau, indicating that the deformation tended toward stability. (3) Accelerated rheological stage: The strain rate increased sharply, the strain–time curve became markedly steeper, and the axial strain rapidly approached the preset termination value.

In the present tests, the attenuated and approximately steady stages were mainly observed at deviatoric stresses of 300 and 600 kPa, whereas the accelerated stage occurred predominantly during the 900 kPa loading stage.

3.2 Axial Rheological Strain under Each Load Level

Based on the curves processed using Chen's method, Table 4 summarizes the mean terminal axial rheological strains obtained from three replicate specimens under each test condition. At the stable load levels of 300 and 600 kPa, axial rheological strain increased progressively with increasing seepage pressure and seepage duration. In contrast, during the third loading stage at 900 kPa, all specimens rapidly reached the preset axial-strain termination criterion of 15% because of accelerated deformation, and exact post-failure strain values were therefore not recorded.

Under the directly measured zero-seepage condition, the mean terminal axial rheological strain was 1.34 ± 0.09% at 300 kPa and 4.77 ± 0.20% at 600 kPa. With increasing seepage intensity and seepage duration, the terminal strain increased substantially. Under the maximum tested seepage condition of 70 kPa and 120 min, the corresponding mean strain reached 3.63 ± 0.25% at 300 kPa and 10.81 ± 0.71% at 600 kPa. These results indicate that seepage markedly enhanced the time-dependent deformation of the tested soil within the stable pre-failure range.

Table 4: Mean terminal axial rheological strains (mean ± SD, n = 3) under each test condition at different deviatoric stress levels.

Condition No.	Seepage Pressure/kPa	Seepage Duration/min	Axial rheological Strain (%)		
			Stage 1 (300 kPa)	Stage 2 (600 kPa)	Stage 3 (900 kPa)
0	0	0	1.34 ± 0.09	4.77 ± 0.20	Not recorded because all specimens reached the preset axial-strain termination criterion (15%).
1	10	48	1.64 ± 0.08	6.35 ± 0.30	
2	10	72	1.68 ± 0.08	6.41 ± 0.31	
3	10	96	1.83 ± 0.10	7.02 ± 0.36	
4	10	120	1.96 ± 0.11	7.26 ± 0.39	
5	30	48	1.76 ± 0.09	6.68 ± 0.34	
6	30	72	1.94 ± 0.11	6.83 ± 0.36	
7	30	96	2.09 ± 0.12	7.37 ± 0.39	
8	30	120	2.28 ± 0.14	7.45 ± 0.40	
9	50	48	2.06 ± 0.12	7.14 ± 0.40	
10	50	72	2.54 ± 0.16	7.78 ± 0.45	
11	50	96	2.66 ± 0.17	8.33 ± 0.50	
12	50	120	2.74 ± 0.18	8.66 ± 0.52	
13	70	48	2.53 ± 0.16	7.52 ± 0.42	
14	70	72	3.08 ± 0.20	8.10 ± 0.47	
15	70	96	3.26 ± 0.22	9.83 ± 0.63	
16	70	120	3.63 ± 0.25	10.81 ± 0.71	

Note: At 900 kPa, all tests were terminated when the axial strain reached 15%; therefore, the recorded observations are termination-limited rather than stable rheological endpoints.

As shown in Fig. 5, the specimen exhibited a relatively intact cylindrical shape before testing. After termination of the 900 kPa loading stage, pronounced axial shortening and lateral deformation were observed. This marked change in specimen appearance, together with the rapid strain development at this load level, indicates that the specimen had entered an accelerated deformation state rather than a stable rheological stage. Accordingly, the 900 kPa data were treated as termination-limited observations rather than stable rheological endpoints. These observations do not represent ultimate post-failure strains and are not directly comparable with the stable terminal strains obtained at 300 and 600 kPa. Consequently, the 900 kPa results were excluded from the subsequent regression analysis and two-way ANOVA.

Accordingly, the subsequent empirical analyses were restricted to the stable pre-failure responses at 300 and 600 kPa within the tested range. A more detailed examination of the individual effects of seepage pressure and seepage duration is presented in Sections 3.3 and 3.4, respectively.

3.3 Influence of Seepage Pressure on Rheological Strain

Figs. 6 and 7 present the replicate measurements, group means with standard deviations, and fitted quadratic trend lines showing the variation in axial rheological strain with seepage pressure at each fixed seepage duration. At both load levels, the axial rheological strain generally increased nonlinearly with increasing seepage pressure.

(**a**) before testing (**b**) after testing

Figure 5: Representative appearances of the specimen before testing and after failure under a deviatoric stress of 900 kPa.

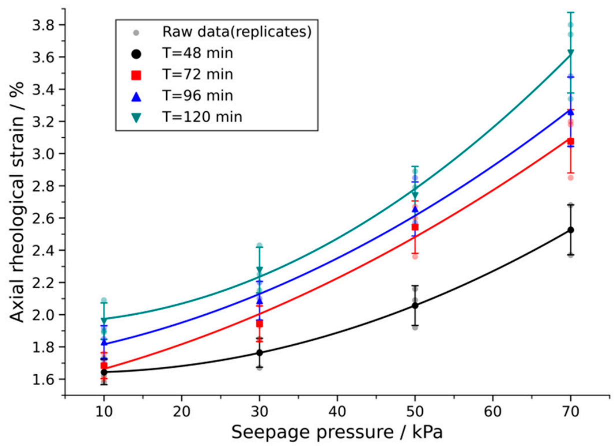

Figure 6: Effect of seepage pressure on axial rheological strain at a deviatoric stress of 300 kPa under different seepage durations. Light-colored points denote individual replicate measurements, symbols with error bars denote the mean ± standard deviation (n = 3), and solid curves denote quadratic fits.

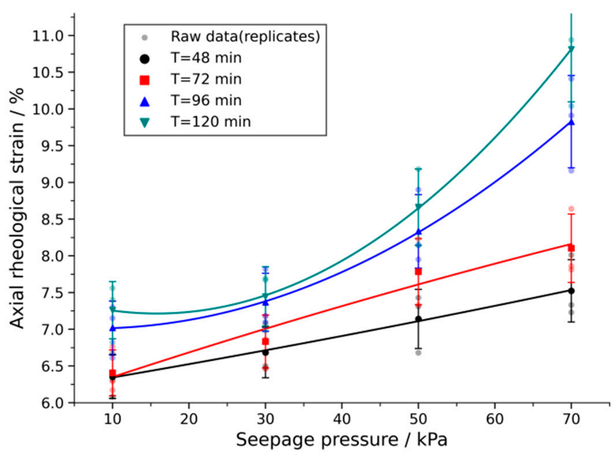

Figure 7: Effect of seepage pressure on axial rheological strain at a deviatoric stress of 600 kPa under different seepage durations. Light-colored points denote individual replicate measurements, symbols with error bars denote the mean ± standard deviation (n = 3), and solid curves denote quadratic fits.

At a deviatoric stress of 300 kPa, the mean terminal axial rheological strain increased from 1.64% to 2.53% when the seepage pressure rose from 10 to 70 kPa at a seepage duration of 48 min, and from 1.96% to 3.63% at a seepage duration of 120 min. At 600 kPa, the corresponding strain increased from 6.35% to 7.52% at 48 min and from 7.26% to 10.81% at 120 min. These results indicate that the promoting effect of seepage pressure on rheological deformation became more pronounced at longer seepage durations, particularly under the 600 kPa load level.

The increasingly steep trends observed at longer seepage durations suggest that the pressure effect did not act independently of seepage duration. Instead, the influence of seepage pressure became stronger as seepage persisted, especially under the higher mechanical load. This pattern is consistent with the later ANOVA results showing a statistically significant interaction between seepage pressure and seepage duration.

From a mechanistic perspective, the enhanced deformation under higher seepage pressure may be associated with increased pore-water pressure, reduced effective confinement, and progressive weakening of the soil skeleton [17]. However, because internal pore-pressure redistribution, particle migration, and local seepage channels were not directly measured in the present study, these mechanisms should be regarded as plausible interpretations of the macroscopic response rather than directly verified processes.

3.4 Influence of Seepage Duration on Rheological Strain

Figs. 8 and 9 present the replicate measurements, group means with standard deviations, and fitted trend lines showing the variation in axial rheological strain with seepage duration at each fixed seepage pressure. At both load levels, the axial rheological strain generally increased with increasing seepage duration, indicating a clear accumulation of time-dependent deformation under sustained seepage.

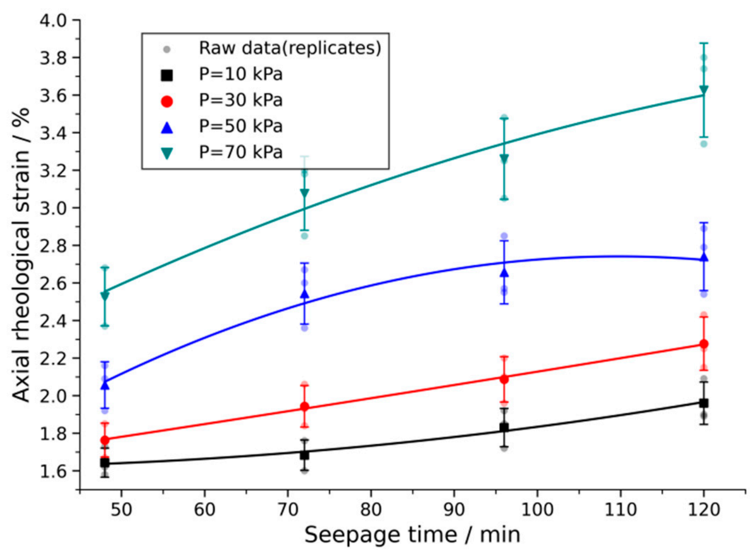

Figure 8: Effect of seepage duration on axial rheological strain at a deviatoric stress of 300 kPa under different seepage pressures. Light-colored points denote individual replicate measurements, symbols with error bars denote the mean ± standard deviation (n = 3), and solid curves denote fitted trends.

At a deviatoric stress of 300 kPa, as the seepage duration increased from 48 to 120 min, the mean terminal axial rheological strain increased from 1.64% to 1.96% at a seepage pressure of 10 kPa and from 2.53% to 3.63% at 70 kPa. At 600 kPa, the corresponding increases were from 6.35% to 7.26% at 10 kPa and from 7.52% to 10.81% at 70 kPa. These results show that the influence of seepage duration became more pronounced at higher seepage pressures, particularly under the 600 kPa load level.

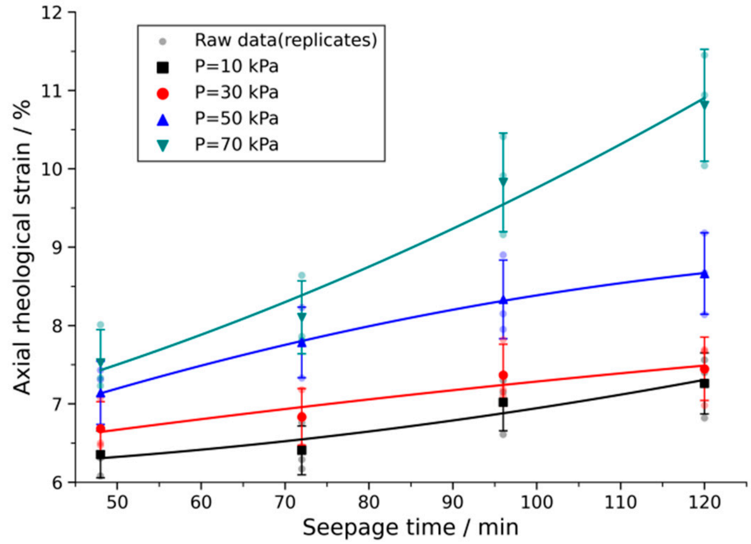

Figure 9: Effect of seepage duration on axial rheological strain at a deviatoric stress of 600 kPa under different seepage pressures. Light-colored points denote individual replicate measurements, symbols with error bars denote the mean ± standard deviation (n = 3), and solid curves denote fitted trends.

The increasingly steep duration-dependent trends at higher seepage pressures indicate that seepage duration did not act independently of seepage pressure. Instead, the duration effect became stronger as the seepage pressure increased. This pattern is particularly evident under the combined condition of 600 kPa deviatoric stress and 70 kPa seepage pressure, where the marked strain increase after 72 min suggests intensified time-dependent deformation under sustained hydraulic disturbance. This observation is consistent with the subsequent ANOVA results showing a statistically significant interaction between seepage pressure and seepage duration.

From a mechanistic perspective, longer seepage duration extends the period over which hydraulic action can weaken the soil skeleton and promote deformation accumulation. Under higher seepage pressure, this sustained hydraulic disturbance may further enhance the susceptibility of the soil to time-dependent strain development. However, because pore-pressure redistribution, hydraulic-conductivity evolution, and particle migration were not directly measured in the present study, these interpretations should be regarded as plausible explanations of the macroscopic response rather than directly verified internal mechanisms.

3.5 Statistical Analysis of Main and Interaction Effects

To quantitatively evaluate the statistical significance and relative contributions of seepage pressure and seepage duration, two-way fixed-effects ANOVA was performed using the replicate-level terminal axial rheological strain data from the complete 4 × 4 factorial matrix. Seepage pressure and seepage duration were treated as fixed factors, each with four levels, and three replicate specimens were tested under each condition. The directly measured zero-seepage control was excluded from the ANOVA because it did not belong to the complete factorial design. The ANOVA results for the 300 and 600 kPa load levels are summarized in Table 5.

Table 5: Two-way ANOVA results for the main and interaction effects of seepage pressure and seepage duration on terminal axial rheological strain.

Load Level	Source	SS	df	MS	F	*p*-Value	Partial η^2
300 kPa	Seepage pressure (P)	12.6640	3	4.2213	185.3997	<0.0001	0.9456
	Seepage duration (T)	2.7345	3	0.9115	40.0335	<0.0001	0.7896
	Interaction ($P \times T$)	0.6127	9	0.0681	2.9899	0.0106	0.4568
	Error	0.7286	32	0.0228	—	—	—
	Total	16.7398	47	—	—	—	—
600 kPa	Seepage pressure (P)	38.4823	3	12.8274	63.6419	<0.0001	0.8565
	Seepage duration (T)	20.1406	3	6.7135	33.3084	<0.0001	0.7574
	Interaction ($P \times T$)	7.7756	9	0.8640	4.2864	0.0010	0.5466
	Error	6.4498	32	0.2016	—	—	—
	Total	72.8482	47	—	—	—	—

Note: Partial η^2 denotes the partial eta-squared effect size.

At 300 kPa, seepage pressure and seepage duration both had highly significant effects on axial rheological strain ($p < 0.0001$), and their interaction was also statistically significant ($p = 0.0106$). The corresponding partial η^2 values were 0.9456 for seepage pressure, 0.7896 for seepage duration, and 0.4568 for the interaction, indicating that seepage pressure contributed the largest proportion of the observed strain variation, followed by seepage duration and then the pressure–duration interaction.

At 600 kPa, the main effects of seepage pressure and seepage duration remained highly significant ($p < 0.0001$), while the interaction became more pronounced ($p = 0.0010$). The partial η^2 values were 0.8565 for seepage pressure, 0.7574 for seepage duration, and 0.5466 for the interaction. These results again identify seepage pressure as the dominant factor within the tested range, while also showing that the relative contribution of the interaction increased under the higher mechanical load.

The statistically significant interaction indicates that the effect of seepage duration depended on the seepage-pressure level and, conversely, that the pressure effect varied with seepage duration. This finding is consistent with the increasingly nonparallel trends observed in Figs. 6–9, where the strain increase associated with one seepage variable became more pronounced as the other variable increased.

As the deviatoric stress increased from 300 to 600 kPa, the partial η^2 values for seepage pressure and seepage duration decreased from 0.9456 to 0.8565 and from 0.7896 to 0.7574, respectively, whereas that for the interaction increased from 0.4568 to 0.5466. Therefore, although seepage pressure remained the dominant factor at both load levels, the pressure–duration interaction became relatively more important under the higher load level. This statistical result provides formal support for the stronger coupled deformation response observed under 600 kPa, especially in the high-pressure and long-duration range.

3.6 Empirical Modeling of the Combined Effects of Seepage Pressure and Seepage Duration

To quantitatively characterize the combined influence of seepage pressure and seepage duration on axial rheological strain, an empirical power-function response-surface model was fitted to the mean terminal strains of the 16 seepage conditions:

$$\varepsilon = a \cdot P^b \cdot T^c + d \tag{1}$$

where ε is the axial rheological strain (%), P is the seepage pressure (kPa), T is the seepage duration (min), a is the seepage-influence coefficient, b is the seepage-pressure exponent reflecting the nonlinear dependence of strain on seepage pressure, c is the seepage-duration exponent reflecting the cumulative influence of seepage duration, and d is the axial rheological strain under the zero-seepage condition. The value of d was fixed at the directly measured mean strain of the zero-seepage control rather than estimated freely during regression. The fitted parameters and model-performance metrics at 300 and 600 kPa are summarized in Table 6.

Table 6: Fitted parameters and performance metrics of the empirical power-function response-surface models.

Model Parameter	Stage 1 (300 kPa)	Stage 2 (600 kPa)
Seepage-influence coefficient a	0.0016	0.0229
Seepage-pressure exponent b	0.9439	0.4837
Seepage-duration exponent c	0.6764	0.7053
Rheological strain under no seepage d	1.3400	4.7700
Fitting degree R^2	0.9488	0.8579
RMSE	0.1310	0.4434
MAE	0.1121	0.3717
LOOCV Q^2	0.9208	0.7371
LOOCV RMSE	0.1630	0.6032
LOOCV MAE	0.1394	0.4835

Note: RMSE, MAE, LOOCV RMSE, and LOOCV MAE are expressed in percentage points of axial rheological strain. LOOCV denotes leave-one-condition-out cross-validation.

At 300 kPa, the fitted parameters were a = 0.0016, b = 0.9439, c = 0.6764, and d = 1.3400, with R^2 = 0.9488, RMSE = 0.1310, and MAE = 0.1121 percentage points. At 600 kPa, the corresponding values were a = 0.0229, b = 0.4837, c = 0.7053, and d = 4.7700, with R^2 = 0.8579, RMSE = 0.4434, and MAE = 0.3717 percentage points. These results indicate that the model provided a good overall description of the pressure–duration dependence of terminal strain, although the fitting performance was lower at 600 kPa than at 300 kPa.

Leave-one-condition-out cross-validation was further used to assess internal predictive stability. In each iteration, the model was fitted using 15 conditions and then used to predict the omitted condition. The LOOCV results yielded Q^2 = 0.9208, RMSE = 0.1630, and MAE = 0.1394 percentage points at 300 kPa, compared with Q^2 = 0.7371, RMSE = 0.6032, and MAE = 0.4835 percentage points at 600 kPa. The lower cross-validation performance at 600 kPa indicates that the smooth power-function surface was less able to capture the stronger local strain increase observed under high seepage pressure and long seepage duration. Consistently, the residuals ranged from −0.2035 to 0.2690 percentage points at 300 kPa and from −0.7983 to 0.7998 percentage points at 600 kPa.

Bootstrap 95% confidence intervals were used to evaluate parameter uncertainty. At 300 kPa, the intervals were 0.0004–0.0046 for a, 0.777–1.158 for b, and 0.539–0.840 for c. At 600 kPa, the corresponding intervals were 0.0084–0.0559 for a, 0.388–0.596 for b, and 0.550–0.866 for c. In addition, a ±10% local sensitivity analysis showed that the mean absolute prediction changes associated with a, b, and c were 0.100, 0.371, and 0.305 percentage points at 300 kPa and 0.293, 0.526, and 0.934 percentage points at 600 kPa, respectively. Within the tested parameter domain, the fitted response was therefore most sensitive to b at 300 kPa and to c at 600 kPa. These sensitivity results depend on the adopted units, fitted parameter values, and tested range and should not be interpreted as universal material properties.

Figs. 10 and 11 illustrate the fitted response surfaces for the combined effects of seepage pressure and seepage duration on axial rheological strain. At both load levels, the fitted surfaces rise continuously with increasing seepage pressure and seepage duration, indicating that increases in either variable were associated with greater rheological deformation. The curved surfaces further demonstrate that the strain response was nonlinear rather than directly proportional to either seepage variable. At 300 kPa, the measured condition means were generally close to the fitted surface, consistent with the relatively high fitting and cross-validation performance. At 600 kPa, larger deviations occurred in the high-pressure and long-duration region, particularly at P = 70 kPa and T = 96–120 min. The fitted surfaces should therefore be interpreted as empirical representations of the overall pressure–duration response within the tested range rather than exact descriptions of every local variation.

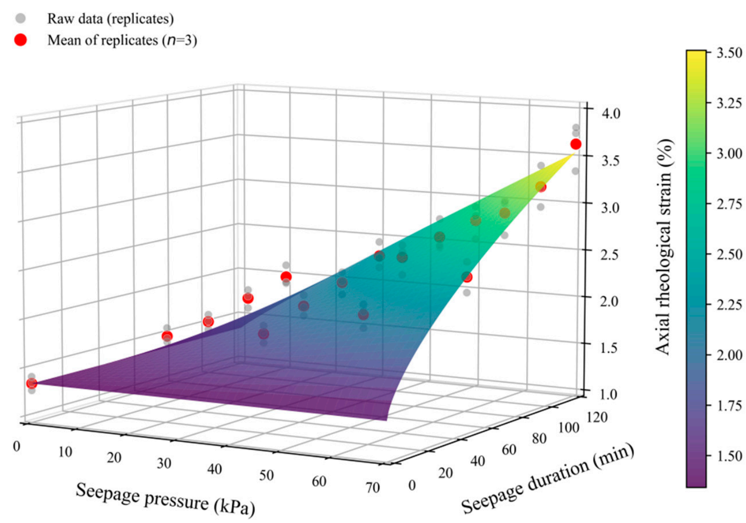

Figure 10: Fitted response surface for axial rheological strain as a function of seepage pressure and seepage duration at 300 kPa.

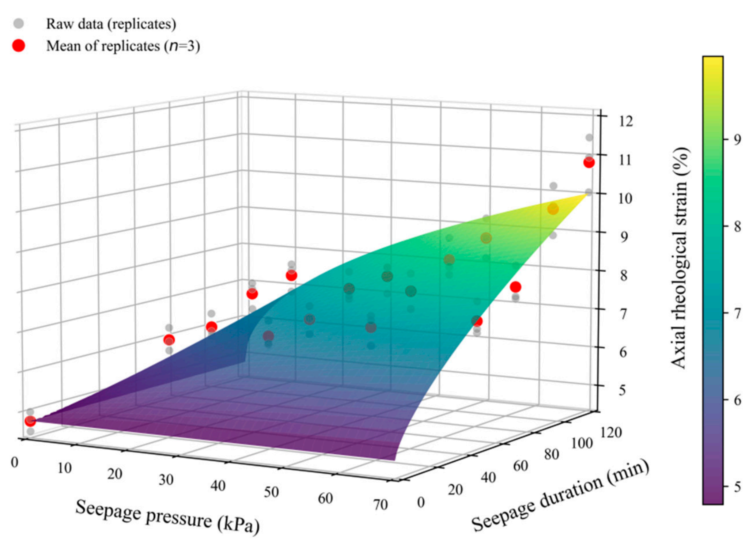

Figure 11: Fitted response surface for axial rheological strain as a function of seepage pressure and seepage duration at 600 kPa.

4 Discussion

4.1 Mechanistic Interpretation of Seepage–Rheology Coupling

The experimental results show that axial rheological strain increased with both seepage pressure and seepage duration, and that their interaction became more pronounced at the higher load level. Within the tested range, seepage pressure exhibited the largest ANOVA effect size at both 300 and 600 kPa, while the relative contribution of the pressure–duration interaction increased at 600 kPa. These findings indicate that the seepage-induced deformation of the tested soil was governed not only by the intensity of hydraulic disturbance, but also by its persistence under sustained loading.

Under a constant cell pressure, increasing seepage pressure may elevate pore-water pressure and reduce the effective confinement acting on the soil skeleton, thereby increasing its susceptibility to time-dependent deformation. In parallel, longer seepage duration extends the period over which hydraulic action can weaken interparticle restraint and promote progressive strain accumulation. The stronger duration effect observed at higher seepage pressures suggests that seepage pressure and seepage duration did not act independently. Instead, their coupled action became more evident as the mechanical load increased, which is consistent with the larger interaction effect identified at 600 kPa.

The pronounced strain increase under high seepage pressure and long seepage duration may also be associated with progressive particle rearrangement, local structural weakening, or fine-particle transport. However, internal pore-pressure redistribution, permeability evolution, seepage velocity, discharged particles, and microstructural changes were not directly measured in the present study. These mechanisms should therefore be regarded as plausible interpretations of the observed macroscopic response rather than processes directly verified by the current experiments.

4.2 Interpretation and Applicability of the Empirical Model

The response-surface model provides a compact quantitative description of the combined effects of seepage pressure and seepage duration on terminal axial rheological strain. In this formulation, the fixed parameter d represents the directly measured zero-seepage response, whereas a, b, and c describe the magnitude of seepage influence and its nonlinear dependence on seepage pressure and seepage duration. The relatively high R^2 and LOOCV Q^2 values indicate that the model captured the overall pressure–duration dependence of terminal strain reasonably well within the tested range, particularly at 300 kPa.

Compared with classical rheological component models such as the Burgers and Nishihara models, the present model serves a different purpose. Classical rheological models are primarily used to describe strain–time evolution under a prescribed loading and hydraulic condition, whereas the present model focuses on the cross-condition coupling among seepage pressure, seepage duration, and terminal strain at selected stable stages. In this sense, the model should be regarded as a compact empirical complement to time-history rheological analysis rather than as a substitute for constitutive modeling.

At the same time, the lower fitting and cross-validation performance at 600 kPa indicates that the smooth power-function surface was less able to capture the stronger local strain increase under high seepage pressure and long seepage duration. The model is therefore most suitable for describing the overall response trend within the tested range, rather than reproducing every local variation exactly.

Because the parameters are condition-dependent and were calibrated only for the present soil, confining pressure, and hydraulic range, the response-surface model should be interpreted as a condition-specific empirical model applicable only within the tested range; it does not describe the 900 kPa failure stage.

4.3 Engineering Implications and Applicability Range

The present results indicate that both seepage intensity and seepage persistence should be considered when evaluating time-dependent deformation in saturated soft-soil excavations. The marked strain increase observed under high seepage pressure and long seepage duration suggests that monitoring strategies should not rely solely on a single hydraulic indicator, such as groundwater-pressure fluctuation, but should also account for the duration of sustained seepage. Under engineering conditions involving heavy rainfall, groundwater-level change, or prolonged seepage exposure, the combined hydraulic effect may be more informative than either parameter considered separately.

Within the tested range, the response-surface model may provide a laboratory-based quantitative reference for identifying unfavorable seepage combinations and supporting comparative deformation assessment. In particular, it may help distinguish relatively mild and relatively severe seepage scenarios for the tested soil under the specified loading conditions. However, the condition of P = 70 kPa and T = 120 min represents only the most severe seepage combination examined in this study, rather than a general rheological-failure threshold.

The present findings were obtained for undisturbed saturated mucky soft soil containing medium-fine sand under a confining pressure of 180 kPa and stable deformation stages at deviatoric stresses of 300 and 600 kPa. Accordingly, the identified deformation trends and model predictions are applicable only within the tested soil type, hydraulic range, and loading conditions. In engineering practice, the results should be used as condition-specific laboratory evidence for monitoring design, comparative risk assessment, and deformation interpretation, rather than as a direct field failure criterion. Application to other soils, confining pressures, stress paths, or unsaturated infiltration conditions requires additional calibration using site-specific tests and field observations.

4.4 Limitations and Future Work

Several limitations should be considered when interpreting the present results. First, the tests were conducted on one undisturbed soil obtained from a single site under saturated conditions and a constant confining pressure of 180 kPa. Therefore, the influences of soil variability, confining pressure, stress path, and unsaturated-to-saturated infiltration were not evaluated. Second, Chen's multistage loading method was applied without paired single-stage verification, and the uncertainty associated with curve conversion may increase near accelerated deformation and failure.

In addition, the present discussion is based mainly on macroscopic strain responses. Internal pore-pressure distribution, seepage velocity, hydraulic-conductivity evolution, discharged particles, and microstructural changes were not directly measured. As a result, the proposed explanations involving structural weakening, particle rearrangement, and fine-particle transport remain inferential and require further experimental verification.

Future work should therefore include a wider range of soil types, confining pressures, and stress paths, together with paired multistage and single-stage loading tests to evaluate conversion accuracy more rigorously. Independent datasets would also be valuable for broader model assessment. Simultaneous measurements of pore pressure, seepage flow, hydraulic conductivity, discharged particles, and microstructure would further clarify the internal processes governing seepage-induced rheological deformation and improve the physical interpretability of the proposed framework.

5 Conclusions

This study investigated the coupled effects of seepage pressure and seepage duration on the rheological response of undisturbed saturated mucky soft soil containing medium-fine sand under a confining pressure of 180 kPa. The main conclusions are as follows:

(1) The processed rheological curves exhibited attenuated, approximately steady, and accelerated stages. Relatively stable rheological deformation was mainly observed at deviatoric stresses of 300 and 600 kPa. At 900 kPa, all specimens rapidly approached the prescribed axial-strain termination criterion; therefore, the results at this stress level characterize rapid failure rather than stable terminal rheological deformation.

(2) Axial rheological strain increased nonlinearly with both seepage pressure and seepage duration. Two-way ANOVA showed that seepage pressure, seepage duration, and their interaction all had statistically significant effects at 300 and 600 kPa. Within the tested ranges, seepage pressure exhibited the largest effect size at both stress levels, while the relative contribution of the pressure–duration interaction increased at 600 kPa. The enhanced deformation under high seepage pressure and long seepage duration indicates a clear hydraulic acceleration effect.

(3) The empirical power-function response-surface model, anchored to the directly measured zero-seepage strain, effectively described the coupled effects of seepage pressure and seepage duration on terminal axial rheological strain. The response-surface model yielded R^2 values of 0.9488 and 0.8579 and LOOCV Q^2 values of 0.9208 and 0.7371 at 300 and 600 kPa, respectively. The response-surface model therefore provides a compact empirical complement to time-history rheological models within the tested stable pre-failure range.

(4) Under the maximum tested seepage condition of 70 kPa and 120 min, the mean axial rheological strain reached 3.63 ± 0.25% at 300 kPa and 10.81 ± 0.71% at 600 kPa. These results demonstrate that the deformation response becomes increasingly sensitive to seepage conditions as the deviatoric stress increases. The reported relationships and response-surface model apply only to the tested conditions and do not describe the 900 kPa failure stage; they should not be interpreted as a universal constitutive law or a general failure criterion.

Acknowledgement: Not applicable.

Funding Statement: This work was supported by the National Natural Science Foundation of China (Grant No. 51278437), the Xiamen Natural Science Foundation Project (Grant No. 3502Z20227323), and projects from the Department of Housing and Urban-Rural Development of Fujian Province (Grant Nos. 2023-K-79, 2023-K-75).

Author Contributions: Longbin Lin: Conceptualization, methodology, investigation, formal analysis, data curation, visualization, and writing—original draft preparation. Hua Hu: Supervision, project administration, funding acquisition, validation, writing—review and editing, and correspondence. All authors reviewed and approved the final version of the manuscript.

Availability of Data and Materials: The data that support the findings of this study are available from the corresponding author upon reasonable request.

Ethics Approval: Not applicable.

Conflicts of Interest: The authors declare no conflicts of interest.

References

1. Lin L, Hu H, Wu Z. Improved Burgers rheological model and identification of rheological parameters for sandy soft soil under seepage conditions. UPB Sci Bull Ser D Mech Eng. 2026;88(1):177–90.
2. Bergado DT, Jamsawang P, Voottipruex P, Jongpradist P, Rementilla J, Dicker S. First and second vacuum-PVD improvement of soft Bangkok clay for the third runway of Suvarnabhumi International Airport Thailand. Innov Infrastruct Solut. 2024;9(9):348. [CrossRef].
3. Puttiwongrak A, Deekaoropkun T, Sin KP, Saowiang K, Jamsawang P, Sukontasukkul P. Basal heave stability analysis of excavations in Bangkok soft clay with confined groundwater recovery using numerical modeling. Modelling. 2025;6(1):21. [CrossRef].
4. Wang S, Zhan Q, Wang L, Guo F, Liu T, Pan Y. Unsaturated creep behaviors and creep model of slip-surface soil of a landslide in Three Gorges Reservoir area, China. Bull Eng Geol Environ. 2021;80(7):5423–35. [CrossRef].
5. Li Y, Song Y, Huang D. Creep behavior and damage constitutive model of sandstone: An experimental study on seepage-load coupling. Mech Time-Depend Mater. 2024;28(4):2751–70. [CrossRef].
6. Reshma B, Viswanadham BVS, Rajagopal K. Centrifuge modeling and piv analysis of geogrid reinforced pile supported embankments over soft clay. Int J Geosynth Ground Eng. 2024;10(4):62. [CrossRef].
7. Frenelus W, Peng H. Evaluating the time-dependent behavior of deeply buried tunnels in soft rock environments and relevant measures guaranteeing their long-term stability. Appl Sci. 2023;13(18):10542. [CrossRef].
8. Ding P, Ju L, Xu R, Yan Z, Wu M, Zhang G. An egg-shaped elastic viscoplastic model for clay: experimental investigation and constitutive modelling. KSCE J Civ Eng. 2023;27(5):1993–2003. [CrossRef].
9. Haji TR, Mir BA. Effect of nano-gypsum on mechanical properties of cement admixed marginal silty soil. Constr Build Mater. 2023;408:133639. [CrossRef].
10. Yaghoubi M, Arulrajah A, Horpibulsuk S. Engineering behaviour of a geopolymer-stabilised high-water content soft clay. Int J Geosynth Ground Eng. 2022;8(3):45. [CrossRef].
11. Tran-Nguyen HH, Luong BT, Nguyen KDT. Investigation of the hydraulic conductivity of soilcrete specimens made by soft clays and medium clays mixed with cement. Geotech Geol Eng. 2023;41(2):1073–82. [CrossRef].
12. Emmanuel E, Anggraini V, Raghunandan ME, Asadi A, Bouazza A. Improving the engineering properties of a soft marine clay with forsteritic olivine. Eur J Environ Civ Eng. 2022;26(2):519–46. [CrossRef].
13. Khalid MH, Yasmin T, Alshameri B, Jamil SM, Hassan W. Comparison of seepage evaluation methods for earth-filled embankments: A case study of Sukian Dyke, Mangla Dam. Model Earth Syst Environ. 2024;10(2):2257–70. [CrossRef].
14. Nourani V, Behfar N, Dabrowska D, Zhang Y. The applications of soft computing methods for seepage modeling: A review. Water. 2021;13(23):3384. [CrossRef].
15. Buathong P, Jongpradist P, Jamsawang P. Performance evaluation of lightweight clay-air foam embankment on soft Bangkok clay: A full-scale test and 3D numerical analysis. Results Eng. 2025;27:105793. [CrossRef].
16. Attari Y, Jostad HP, Grimstad G, Eiksund GR. Evaluation of pile driving effects on slope stability in clay. Geotech Geol Eng. 2024;42(3):1623–38. [CrossRef].
17. Lei H, Feng S, Jia R, Jiang M. Experimental investigation of the deformation characteristics of Tianjin clays under coupled dynamic stress and seepage fields. Adv Civ Eng. 2019;2019:3785937. [CrossRef].
18. Tan J, Shen Z, Xu L, Zhang H, He Y. Experimental investigation on seepage characteristics of clay–structure interface after shear deformation. Materials. 2022;15(11):3802. [CrossRef].
19. Su J, Wang S. Experimental study on creep characteristics of saturated sandy soil with different fines content. IOP Conf Ser Earth Environ Sci. 2021;719(4):042070. [CrossRef].
20. Cui P, Cao W, Xu Z, Li H, Hu M. One-dimensional nonlinear rheological consolidation analysis of soft ground under continuous drainage boundary conditions. Comput Geotech. 2023;156:105283. [CrossRef].
21. Qi J, Xie Y, Li C, Guo H, Wang Y. Creep behavior of clayey soil and its model prediction in the Cangzhou land subsidence area. Sci Rep. 2025;15:9130. [CrossRef].
22. Liu Y, Fang N, Zheng Y, Wu K, Chen R, Lu H, et al. Creep behavior and quantitative prediction of marine soft clay based on a nonlinear elasto-plastic-viscous element assembly model. J Mar Sci Eng. 2025;13(6):1142. [CrossRef].
23. Gong X, Liu Y, Li Q, Ma Y, Zhai M, Ma D, et al. Experimental and numerical study on seepage-creep coupling characteristics of fault rocks. Front Earth Sci. 2025;13:1566556. [CrossRef].

24. Shen Z, Yang K, Wei D, Liang Q, Ma Z, Wang H, et al. Deep learning-based prediction of seepage flow in soil-like porous media. Fluid Dyn Mater Process. 2025;21(11):2741–60. [CrossRef].
25. Liu T, Dai K, Ren S, Zhang C, Tang X, Hu J, et al. Sand production in unconsolidated sandstone: Experimental analysis of multiphase flow during cyclic injection and production. Fluid Dyn Mater Process. 2025;21(12):2981–95. [CrossRef].
26. Liu X. An introduction to rock rheology. Beijing, China: Geological Publishing House; 1994. (In Chinese).
27. Ruan YF, Zhu SW, Qiao WJ, Wu L, Cai L. Creep characteristics of lacustrine sedimentary peaty soil. Chin J Geotech Eng. 2022;44(S1):166–71. (In Chinese). [CrossRef].
28. Yuan JH, Wang YZ, Wang X, Chen YP, Gong XL, Chen T. Experimental and numerical simulation studies on creep behavior of soda residue soil. China Civ Eng J. 2024;57(5):107–16. (In Chinese). [CrossRef].